Acta Biomaterialia 145 (2022) 172–184

Contents lists available at ScienceDirect

Acta Biomaterialia

journal homepage: www.elsevier.com/locate/actbio

Full length article

pH-responsive silica nanoparticles for the treatment of skin wound infections

Fei Pan[a,1], Giorgia Giovannini[b,1], Sixuan Zhang[a], Stefanie Altenried[a], Flavia Zuber[a], Qian Chen[c], Luciano F. Boesel[b], Qun Ren[a,*]

[a] Empa, Swiss Federal Laboratories for Materials Science and Technology, Laboratory for Biointerfaces, Lerchenfeldstrasse 5, St. Gallen 9014, Switzerland
[b] Empa, Swiss Federal Laboratories for Materials Science and Technology, Laboratory for Biomimetic Membranes and Textiles, Lerchenfeldstrasse 5, St. Gallen 9014, Switzerland
[c] Jiangsu Key Laboratory for Carbon-Based Functional Materials and Devices, Institute of Functional Nano & Soft Materials (FUNSOM), Soochow University, Suzhou 215123, China

ARTICLE INFO

Article history:
Received 14 January 2022
Revised 15 March 2022
Accepted 6 April 2022
Available online 10 April 2022

Keywords:
pH-response
Controlled drug release
Silica nanoparticles
Smart wound dressing
Skin wound infection
Antibiotic resistance
Ex vivo skin model

ABSTRACT

Chronic wounds are not only a burden for patients but also challenging for clinic treatment due to biofilm formation. Here, we utilized the phenomenon that chronic wounds possess an elevated local pH of 8.9 and developed pH-sensitive silica nanoparticles (SiNPs) to achieve a targeted drug release on alkaline wounds and optimized drug utility. Chlorhexidine (CHX), a disinfectant and antiseptic, was loaded into SiNPs as the model drug. The loaded CHX displayed a release 4 - 5 fold higher at pH 8.0 and 8.5 than at pH 6.5, 7.0 and 7.4. CHX-SiNPs furthermore exhibited a distinctive antibacterial activity at pH 8.0 and 8.5 against both Gram-negative and -positive bacterial pathogens, while no cytotoxicity was found according to cell viability analysis. The CHX-SiNPs were further formulated into alginate hydrogels to allow ease of use. The antibacterial efficacy of CHX-SiNPs was then studied with artificial wounds on *ex vivo* human skin. Treatment with CHX-SiNPs enabled nearly a 4-lg reduction of the viable bacterial cells, and the alginate formulated CHX-SiNPs led to almost a 3-lg reduction compared to the negative controls. The obtained results demonstrated that CHX-SiNPs are capable of efficient pH-triggered drug release, leading to high antibacterial efficacy. Moreover, CHX-SiNPs enlighten clinic potential towards the treatment of chronic wound infections.

Statement of significance

A platform for controlled drug release at a relatively high pH value *i.e.*, over 8, was established by tuning the physical structures of silica nanoparticles (SiNPs). Incorporation of chlorhexidine, an antimicrobial agent, into the fabricated SiNPs allowed a distinctive inhibition of bacterial growth at alkaline pHs, but not at acidic pHs. The efficacy of the SiNPs loaded with chlorhexidine in treating wound infections was further validated by utilizing *ex vivo* human skin samples. The presented work demonstrates clinic potential of employing alkaline pH as a non-invasive stimulus to achieve on-demand delivery of antimicrobials through SiNPs, showcasing a valuable approach to treating bacterial infections on chronic wounds.

1. Introduction

Skin, the largest organ and first body defense, is divided into two main layers: epidermis and dermis. While the external epidermis has mainly a protective role, the underneath dermis hosts blood and lymphatic vessels, sweat glands, and air follicles [1]. When the dermis is injured, the dynamic physiological process of healing is automatically activated [2]. However, bacterial infections and biofilm formation on the injured wounds may cause chronic or non-healing wounds due to the reinforced resistance towards host defense and antimicrobials [3–5]. Chronic wounds bring notorious suffering to patients and therefore represent a huge concern for global public health regarding the high incidence rate, probable long hospitalization, and the risk of developing complications

* Corresponding author.
E-mail address: Qun.Ren@empa.ch (Q. Ren).
[1] These authors contributed equally to this work.

https://doi.org/10.1016/j.actbio.2022.04.009

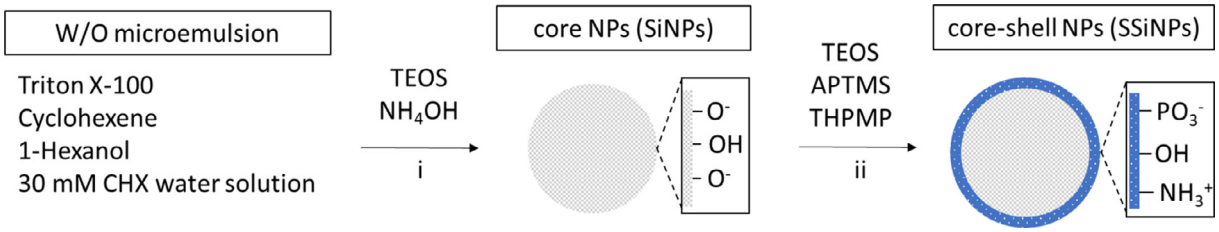

Scheme 1. Scheme of the nanoparticles synthesis. (i) Formation of the TEOS-based silica core; (ii) formation of the outer silica shell with the addition of phosphate and aminopropyl groups using silane derivatives, THPMP and APTMS, respectively.

[6,7]. However, the prevailing application of antibiotics against bacterial infections usually leads to overuse or misuse, subsequently causing the emergence of antimicrobial resistance [8]. The main goal of wound management is to prevent bacterial colonization with optimized treatment, ultimately favoring the wound healing process. In the last decade, many efforts have been dedicated to developing new dressing bearing antibacterial properties and capable of stimulating wound healing. However, the gold standard is still represented by the local application of silver sulfadiazine-based medical aids, which can cause cytotoxic problems. Considering that the local wound pH can rise to as high as 8.9 once chronic wounds are formed [9], wound dressing sensitive to an alkaline scenario is highly advantageous for targeted treatment of bacterial infections on chronic wounds and optimizing utilization of antimicrobials.

Nanomaterials are widely applied in drug delivery thanks to their advantageous properties (*e.g.,* surface/volume ratio, loading capacity, surface functionalization). In particular, incorporating a drug into nanocarriers improves the bioavailability of poorly soluble drugs and protects them from inactivation in biological conditions [10–13]. Moreover, with a rational selection of nanocarriers of different physicochemical characteristics, the drug can be released in response to specific stimuli and in a controlled manner depending on the targeted application. Controlled zero-order release of drugs from nanoparticle systems has been intensively investigated [14]. Stimuli-dependent (pH, temperature, light, ionic strength, et al. [5,15–17]) release sustains the amount of the drug in the therapeutic window and ultimately improves both the efficacy of the treatment and the patient's compliance [5,18,19].

Among those functional materials developed for a smart drug delivery, silica nanoparticles (SiNPs) have gained special attention due to their straightforward synthesis, uniform morphology, controllable diameter, modifiable surface charge, feasible functionalization, and significant biocompatibility [20–23]. SiNPs moreover display a variety of physicochemical properties, such as different porosity, charge, and hydrophobicity, enabling various encapsulation of different kinds of therapeutics and related delivery to the desired sites [22]. In particular, SiNPs can be designed with a defined kinetic of drug release in response to specific environmental stimuli thanks to many commercially available siloxane derivatives [22]. In contrast to mesoporous SiNPs (pore size of the order: 2–50 nm) requiring a post-synthesis for drug loading (pore size < 2 nm), the encapsulation of molecules by microporous SiNPs can be achieved during NPs synthesis [24]. Moreover, the release mechanism concerning microporous SiNPs is a simple diffusion of the loaded compounds or a degradation of the silica matrix, which can therefore be regulated by changing the siloxane precursors [25]. Hence a controlled release of encapsulated drug can be obtained from microporous SiNPs by synthesizing colloids through applying different organosiloxane precursors.

In this work, we designed and fabricated pH-responsive silica nanoparticles, which can be triggered for a high release of antimicrobials at a relatively high pH value of over 8. Two different structures of silica nanoparticles were first fabricated, one with an additional outer shell (SSiNPs) and one without (SiNPs) (Scheme 1). Chlorhexidine (CHX, an efficacious skin antiseptic [26,27]) was herein utilized as a model drug and incorporated into the silica nanoparticle system. The fabricated silica nanoparticles were optimized for their pH-triggered release by tuning the physical structures. The CHX-SiNPs were revealed to display a distinctive inhibition of bacterial growth at alkaline pHs, whereas CHX-SSiNPs did not. Furthermore, the pH-regulated release dramatically reduced viable bacteria on artificial wounds by exploiting *ex vivo* human skin. To the best of our knowledge, it has not been exploited to utilize alkaline pH as a stimulus for a controlled antibacterial activity, which was confirmed with artificial wounds on *ex vivo* human skin. These achievements demonstrate that CHX-SiNPs pose a promising application for the treatment of chronic wounds.

2. Experimental procedures

2.1. Materials

Cyclohexane (anhydrous, 99.5%), 1-hexanol (anhydrous, $\geq$ 99%), Triton® X-100, 3-(trihydroxysilyl)propyl methylphosphonate monosodium salt (42% w/v in water) [THPMP], aminopropyl trimethoxysilane [APTMS] (97%), tetraethyl orthosilicate [TEOS] (99.99%), ammonium hydroxide solution (28% w/v in water, $\geq$ 99.99%), alginate sodium salt, calcium chloride, dimethyl sulfoxide anhydrous, $\geq$ 99.9% (DMSO), fluorescein isothiocyanate (FITC), sodium phosphate dibasic ($>$ 98.5%), sodium phosphate monobasic ($>$ 98%), and absolute ethanol. These chemicals and reagents of analytical purity were ordered from Sigma-Aldrich (Buchs, Switzerland) and applied as received unless otherwise noticed. *Ex vivo* human skin samples were provided by Cantonal Hospital St. Gallen, with anonymous consent from the donors and exempted from ethical approval.

2.2. Fabrication of SiNPs, SSiNPs, drug-loaded SiNPs (CHX-SiNPs), and drug-loaded SSiNPs (CHX-SSiNPs)

For the preparation of SiNPs, a slightly modified protocol based on the microemulsion quaternary method has been utilized [28]. Briefly, 30 mM chlorhexidine (CHX) suspension was prepared by firstly dissolving CHX in 0.3 mL DMSO and then adding dropwise deionized (DI) water under stirring till reaching the desired concentration of 30 mM. This process resulted in dissolution of 40 mg CHX in a final volume of 2.6 mL. The solution was subsequently stirred overnight at room temperature. SiNPs were formed in microemulsion prepared by combining 7.5 mL cyclohexane, 1.133 mL 1-hexanol, 1.894 g Triton X-100 and 0.48 mL prepared chlorhexidine suspension in a 30 mL plastic bottle under constant stirring. To form the silica core, 100 µL of TEOS were added to the mixture. Thirty minutes later, 40 µL of ammonium hydroxide (28% $w \cdot v^{-1}$) was also added to trigger polymerization. After 24 h, the microemulsion was destabilized by introducing 30 mL ethanol. The

fabricated NPs were then purified three times by centrifugation (1189 g, 10 min) and re-dispersion. They were firstly re-dispersed in ethanol, secondly in diluted ethanol by DI water (50%), and thirdly in DI water.

SSiNPs and CHX-SSiNPs were formed by introducing an additional outer shell onto SiNPs and CHX-SiNPs after the trigger polymerization of 24 h. 40 µL THPMP was then added into the mixture for a reaction of 20 min; subsequently, 50 µL TEOS was added, and 5 min later, 10 µL APTMS was introduced. After a further stirring of 24 h, a similar break of microemulsions and a purification of NPs were conducted as aforementioned.

All the produced nanoparticles were stored at 4 °C in DI water. Reference samples, SiNPs and SSiNPs, were prepared by simply adding DI water (0.48 mL) instead of the chlorhexidine suspension during micro-emulsion preparation.

2.3. Labeled SiNPs embedded in alginate hydrogel

Core-SiNPs were synthesized following the same procedure as CHX-SiNPs, but the loaded drug was replaced by 54 µM fluorescein isothiocyanate (FITC). FITC-SiNPs were mixed with alginate (3% wt) with a final concentration of 330 mg·L^{-1}, and the hydrogels were formed by adding 0.1 mL of 5% wt $CaCl_2$. Both leakage and SiNPs degradation were evaluated by measuring the fluorescent signal of FITC ($\lambda_{excitation}$: 490 nm, $\lambda_{emssion}$: 517 nm) in the supernatant after incubation at various conditions (*i.e.*, 0.5 mL of water or PBS at pH 6.0, 7.0, and 8.0). The analysis was accomplished in triplicates. The amount of FITC was defined using the corresponding calibration curve of FITC at pH 6, 7, and 8, and it is reported as the percentage of the amount used for the sample formation. All spectra were recorded using Varian Cary Eclipse (Agilent Technologies, U.S.A.). Fluorescent images were acquired by employing a laser scanning confocal microscope (LSM 780, Zeiss, Germany) LASOS Ar-lon Laser (Model LGN 3001, Remote Control RMC 7812 Z2, 490 nm, Zeiss, Germany).

2.4. NPs embedded in alginate hydrogel

A 3% wt sodium alginate solution (AH) was prepared by dissolving the powder in DI water at 60 °C. After cooling, CHX-SSiNPs, CHX-SiNPs, SSiNPs, and SiNPs were added to 0.1 mL of sodium alginate solution for a final NPs concentration of 330 mg·L^{-1}. The samples were placed in a mold (96 well plate) after vortexing, and 0.1 mL of 5% wt $CaCl_2$ was then added. One hour later, the fabricated hydrogels (SiNPs@AH, CHX-SiNPs@AH, SSiNPs@AH, and CHX-SSiNPs@AH) were washed with DI water and applied in the antibacterial assay.

2.5. Transmission electron microscopy (TEM)

TEM analysis was performed by utilizing a JEOL TEM equipped with an in-column Omega-type energy filter (JEM-2200FS, Joel, Japan). 5 µL of NPs in water (20 mg·L^{-1}) was added onto a TEM grid (Carbon Film Supported Copper Grid, 200 Meshes, Electron Microscopy Sciences, USA) till it was completely evaporated. ImageJ software (National Institutes of Health, U.S.A.) was applied to conduct a statistical analysis of the imaged *circa* 50 NPs.

2.6. Dynamic light scattering (DLS) and zeta potential

The sizes and zeta potentials of the fabricated NPs were measured by Zetasizer NanoZS (Malvern Instruments Ltd, Malvern, UK) through a HeNe laser of 633 nm with a backscatter angle of 90°. SiNPs, CHX-SiNPs, SSiNPs, and CHX-SSiNPs were diluted to a final concentration of 20 µg·mL^{-1} in DI water. 1.5 mL disposable plastic cuvettes were used to measure the size and polydispersity index (PDI), while ζ-potential measurement was accomplished using disposable folded capillary cell (DTS1070, Malvern Instruments Ltd, Malvern, UK). The parameters applied in the measurements were room temperature (~25 °C), dispersant viscosity of 0.8872 cP, reflective index of 1.330, the material of absorption 0.01, and refractive index of 1.49. The final average values were reported through three measurements.

2.7. Fourier-transform infrared spectroscopy (FTIR)

FTIR analysis was performed through a Bruker FTIR operating in attenuated total reflectance (TENSOR-27, Bruker, Germany). FTIR spectra were recorded and analyzed in a range of 1300–2200 cm^{-1} with a resolution fixed to 2 cm^{-1}.

2.8. Thermogravimetric analysis (TGA)

TGA was carried out with 2.0–4.0 mg samples by utilizing a thermogravimetry (TG-209 F1 Iris, Netzsch, Germany) in N_2 and air with a heating rate of 1 °C·min^{-1} from 21 °C to 80 °C.

2.9. In vitro *drug release kinetics*

SiNPs and SSiNPs loaded with CHX were centrifuged at 2150 g for 5 min, and PBS buffers subsequently replaced the supernatant at pHs of 6.5, 7.0, 7.4, 8.0, and 8.5. 1 mL 330 mg·L^{-1} each NPs were subsequently and, respectively pipetted to a 1.5 mL Eppendorf tube for CHX release analysis after 0, 0.15, 0.5, 1, 2, 6, 8, 24 30 h. All the Eppendorf tubes were incubated at 37 °C and shaken at 30 rpm. At the due time, the corresponding Eppendorf tubes were centrifuged at 2150 g for 5 min. 50 µL of the supernatant were then analyzed by a UV-visible spectrophotometer (PowerWave HT, BioTek Instruments Inc, USA) to quantify the CHX release at a wavelength of 265 nm. The corresponding release amount of CHX was determined with a standard calibration curve (Fig. S2). Drug loading efficiency was calculated through the ratio of the concentration of CHX released from NPs at pH 9.0 for two weeks to the concentration of the NPs loaded with CHX.

2.10. Degradation analysis by TEM

CHX-SiNPs and CHX-SSiNPs were re-dispersed in PBS buffers at different pHs (6.5 and 8.5) at a concentration of 200 mg·L^{-1}. For every buffer, 4 samples were prepared, one for every time point (2, 6, 8, and 24 h) and shaken at 37 °C (600 rpm). After every incubation, samples were centrifuged (1189 g, 10 min). The supernatant was discarded, and the pellet isolated was washed twice by centrifugation and re-dispersion in water to remove salts. Subsequently, it was re-dispersed in 100 µL DI water. 5 µL final suspension of every sample was then dropped onto TEM grids for observation.

2.11. Antibacterial assay

Escherichia coli DSMZ 22312 and *Staphylococcus aureus* ATCC 6538 were utilized in the antibacterial assay. One bacterial colony from an agar plate was incubated in 10 mL LB media in 15 mL Falcon tubes at 160 rpm and 37 °C overnight. 100 µL overnight culture was pipetted into 10 mL fresh LB media and cultivated for around 2 h till exponential growth. The bacterial cultures of *E. coli* and *S. aureus* were diluted with sterile PBS as reported [29,30] to 10^6 (OD_{600} 0.01) colony forming units (CFU)·mL^{-1}. 200 µL of bacterial suspension (*circa* 10^6 CFU·mL^{-1}) was then thoroughly spread on BHI agar plates. One hour later, 10 µL 500 mg·L^{-1} CHX solution and its 10 times diluted solution, 330 mg·L^{-1} SiNPs, 330 mg·L^{-1} CHX-SiNPs, 330 mg·L^{-1} SSiNPs, and 330 mg·L^{-1} CHX-SSiNPs were sub-

sequently pipetted four times on bacterial spread BHI agar plates. All plates were incubated at 37 °C for 10 h. Images of BHI agar plates were subsequently taken after overnight incubation to obtain a qualitative analysis of inhibition of bacterial growth of every sample.

In vitro antibacterial assay was quantitatively analyzed in PBS at pH 6.5, 7.0, 7.4, 8.0, and 8.5. 100 µL bacterial suspensions (OD_{600} 0.1) at every pH condition was added to 1 mL 330 mg·L^{-1} NPs (SiNPs, SSiNPs, CHX-SiNPs, and CHX-SSiNPs) samples, 1 mL PBS buffer (negative control), and 1 mL 500 mg·L^{-1} CHX solution (positive control), and incubated for two hours. A serial dilution of the suspensions was performed. Subsequently, 100 µL bacterial suspension from every sample was plated on a BHI agar plate with 3 replicates using an automatic plater (easySpiral, interscience, France). Bacterial colonies were counted by a colony counter (Scan® 300, interscience, France) after incubation of roughly 10 h.

2.12. Antibacterial activity investigated with ex vivo human skin samples

Ex vivo human skin models were utilized to analyze the antibacterial efficacy of the fabricated SiNPs, SSiNPs, CHX-SiNPs, and CHX-SSiNPs, and alginate hydrogels encapsulated with these NPs. The infected wounds treated with 500 mg·L^{-1} CHX solution were used as the positive control, and the ones treated with PBS buffer were as the negative control. Artificial burn wounds were generated by applying a stamp (diameter 10 mm, heated to 200 °C) for 5 s on human skins, obtained from Cantonal Hospital St.Gallen, and pre-treated by cutting the excessive fat. The artificial burn wounds were subsequently punched at a diameter of 20 mm. These artificial burn wounds were then washed sequentially with octenidine dihydrochloride (octenisept® farblos/incolore, Schülke & Mayr GmbH) for 5 min and three times with Dulbecco's PBS (every time for 10 min). The sterilized wounds were placed in TPP 6-well plates with 600 µL DMEM (Dulbecco's Modified Eagle Medium) containing 10% foetal calf serum (FCS). 20 µL bacterial suspension (10^6 CFU·mL^{-1}) was loaded onto the wound and incubated at 37 °C for 24 h. Subsequently, 20 µL 330 mg·L^{-1} NPs samples and control samples, and the NPs-formulated alginate hydrogels were loaded on the wound surfaces, followed by an incubation for 2 h at 37 °C. The wounds were transferred into 15 mL TPP tubes and ultrasonicated with 5 mL PBS for 1 min. After a serial dilution of the suspensions, 100 µL bacterial suspension was plated on a BHI agar plate using an automatic plater (easySpiral, interscience, France). Bacterial colonies were counted by a colony counter (Scan® 300, interscience, France) after incubation at 37 °C for roughly 10 h.

Ex vivo human skin samples were obtained from Cantonal Hospital St. Gallen, with anonymous consent given by the donors and exempted from ethical approval. Mechanical wounds (5 mm in diameter) were artificially generated on *ex vivo* human skin (13 mm in diameter). Subsequently, the samples were disinfected by octenisept for 5 min and washed with fresh PBS three times and every time for 10 min. The cleaned samples were placed in 12-well plates (TPP Techno Plastic Products AG, Trasadingen, Switzerland) and every well containing 400 µL DMEM (+10% FCS). 20 µL *E. coli* (10^6 CFU mL^{-1}) suspension was loaded on every wound. These samples were incubated at 37 °C under 5% CO_2 for three days. 20 µL 330 mg·L^{-1} CHX-SiNPs samples and CHX-SiNPs formulated alginate hydrogels were loaded onto these infected samples. After 2 h at 37 °C, the samples treated by CHX-SiNPs and alginate hydrogels formulated with CHX-SiNPs were rinsed with PBS buffer and then immersed into fresh 4% formalin for 24 h at 4 °C. The bacteria on wounds were further analyzed by histological staining.

2.13. Histological staining

Histological staining [31,32] was further performed to observe bacteria on the wounds. The samples were transferred into a fresh 12-well plate and rinsed with deionized water for 45 min, and then dehydrated by incubation in increasing ethanol concentrations, rinsed in xylene, and placed in paraffin blocks. 5 µm thick sections were then vertically cut, subsequently deparaffinized in xylene and rehydrated in decreasing ethanol concentrations. The samples were then stained by hematoxylin (HistoLab, Askim, Sweden) and eosin, and rinsed in distilled water between the two steps.

2.14. Cytotoxicity assay

Cytotoxicity of the nanoparticles was studied employing normal human dermal fibroblasts (nHDFs, female, caucasian, skin/temple, PromoCell, C-12352). Nanoparticles (CHX-SiNPs, final concentration: 330 mg·L^{-1} as 0 dilution) were centrifuged at 2150 g for 5 min, and the pellet was resuspended with Dulbecco's Modified Eagle Medium at pH 7.4, 8.0, and 8.5 containing 1% penicillin/streptomycin/neomycin (PSN). A negative control (empty wells) and additional dilutions (2X, 4X, 8X, 16X, 32X, 64X, and 128X) of nanoparticles were in parallel analyzed. nHDFs were preseeded with 10 000 cells per well (TPP, Trasadingen, Switzerland) in 100 µL DMEM containing 10% foetal calf serum (FCS) for 24 h, and then incubated for 24 h with 100 µL 95% nanoparticle solutions diluted with FCS. The viable nHDFs cells of negative control were set as 100%, and the ones incubated with 1% Triton X-100 in DMEM containing 5% FCS were regarded as the positive control. Cell viability was investigated through a MTS [(3-(4,5-Dimethylthiazol-2-yl)-5-(3-carboxymethoxyphenyl)-2-(4-sulfophenyl)-2H-tetrazolium)] assay via the absorbance at 490 nm to determine metabolic activity of the nHDFs [33]. DMEM at pH 8.0 and 8.5 were adjusted by adding sterile NaOH solution.

2.15. Statistics

Statistical differences between nanoparticles were evaluated by applying unpaired and two-tailed student's *t*-test for comparison between two groups.

3. Results and discussion

3.1. Fabrication of CHX-SiNPs and CHX-SSiNPs

Aiming at a pH-responsive drug delivery system, SiNPs and SSiNPs were synthesized by the reverse microemulsion method and loaded with CHX during the synthesis, without an additional post-synthesis as required by other procedures [34]. The pH-dependent degradation of SiNPs was well studied as reported [22]. Usually, the microemulsion procedure leads to the formation of a silica shell obtained by combining silane derivatives, such as the negatively charged 3-(trihydroxysilyl)propyl methylphosphonate (THPMP) and the reactive aminopropyl trimethoxysilane (APTMS). The colloidal suspension achieved with core-shell-SiNPs are usually more stable owing to the counterbalance of positive and negative charges that limits their agglomeration/aggregation. Furthermore, the primary amine can be used in the formulation of the shell to anchor specific molecules on the nanoparticle surface. However, such a shell protects the silica core of the nanoparticles from the environment, potentially slowing down its degradation. We hypothesized that in the absence of a protective shell, the pristine silica-based matrix is more exposed to the environment and thus more susceptible to pH-dependent degradation even in a stable environment (*e.g.*, patches). The different pH susceptibilities of NPs

Table 1
DLS and TEM analysis of the synthesized NPs. 20 mg·L^{-1} SiNPs, CHX-SiNPs, SSiNPs, and CHX-SSiNPs were dispersed in filtered deionized water for DLS analysis. Data are expressed as mean +/- standard deviation (n = 3). The average diameters and the calculated standard deviations of NPs measured by TEM were generated based on an analysis of 100 NPs with ImageJ.

Sample name	DLS analysis			TEM analysis
	Size/nm	Polydispersity Index (PDI)	ζ -potential/ mV	Size/nm
SiNPs	189 +/- 60	0.07	-29.2 +/- 2.8	111 +/- 17
CHX-SiNPs	227 +/- 85	0.16	-33.3 +/- 1.1	102 +/- 19
SSiNPs	207 +/- 94	0.23	-35.9 +/- 1.4	56 +/- 7 (64%) 136 +/- 24 (36%)
CHX-SSiNPs	247 +/- 91	0.33	-36.8 +/- 0.9	59 +/- 8 (57%) 146 +/- 22 (43%)

with and without outer shells are schematized in Scheme 1. Due to the additional outer shell, the loaded drug can hypothetically be better confined inside SSiNPs than SiNPs. To investigate this hypothesis and aim at achieving a sustained drug release, we synthesized both CHX loaded core-shell-SiNPs (SSiNPs) and core-SiNPs (SiNPs) by microemulsion method and compared the kinetics of drug release in response to the varying surrounding environment.

3.2. Physical and chemical characterizations of the CHX-SiNPs and CHX-SSiNPs

One of the advantages in using nanoparticles to develop responsive drug delivery systems is the high surface-to-volume ratio that can be achieved by decreasing the diameter of nanoparticles. The morphology of pristine and CHX-loaded SSiNPs and SiNPs was characterized by dynamic light scattering (DLS) and transmission electron microscopy (TEM). DLS analysis indicated that the loading of CHX led to an increase in the hydrodynamic diameter from 188.8 +/- 60.0 nm to 226.8 +/- 85.0 nm compared to the pristine equivalent. However, such observation was not confirmed by the TEM analysis, where a similar diameter of about 100 nm was observed for all types of particles. The discrepancy observed in the diameter of the particles measured by DLS and TEM was ascribed to the different conditions required by the two measurement techniques. Since DLS analysis requires a NPs suspension, it estimates the hydrodynamic diameter of the particles, including the core and any molecule associated with the surface such as ions and solvent/water molecules. In contrast, TEM images the dehydrated nanoparticles without any associated molecules. The large polydispersity Index (PDI) measured by DLS for SSiNPs and CHX-SSiNPs suggested the presence of different populations in the samples (Table 1). Such heterogeneity was confirmed by the TEM analysis (Fig. 1a), which clearly showed the presence of two different populations for SSiNPs (56.6 +/- 7.1 nm, 64% and 135.9 +/- 24.0 nm, 36%) and CHX-SSiNPs (59.0 +/- 8.0 nm, 57% and 146.3 +/- 22.0 nm, 43%). The presence of two populations in the core-shell samples was related to the nucleation and growth process that occurred after seeding into the microemulsion droplets during the shell formation [35]. These analyses confirmed that the incorporation of the CHX did not affect the size of the nanoparticles. It has been documented that the microorganism-nanoparticle interaction is strongly influenced by electrostatic interactions, hence the surface charge of nanomaterial can determine the antibacterial activity of nanomaterials [36]. Therefore, we further characterized the surface properties and composition of the synthesized nanoparticles. The surface charge was determined by electrophoretic light scattering (ELS), showing that shelled SiNPs were slightly more negatively charged than SiNPs and that the loading of CHX led to a more negative surface. The influence of CHX was more evident in the case of SiNPs, for which the ζ-potential dropped from -29.2 +/- 2.8 (SiNPs) to -33.3 +/- 1.1 (CHX-SiNPs), caused by the cationic property of CHX that leads to the deprotonation of the hydroxyl groups of the TEOS-based matrix [37]. Overall, ELS analysis confirmed that the nanomaterials tested in this study had a comparable surface charge (*ca.* -30 mV). Fourier-transform infrared (FTIR) analysis (Fig. 1b) manifested the band of N-H bending mode in secondary aromatic amine at 1519.80 cm^{-1}, C=N at 1610 cm^{-1}, characteristic bands of C=N stretching vibrations modes in 1690–1640 cm^{-1} and stretching vibrations of C=C group in 1670 - 1626 cm^{-1}, typically for CHX, as previously reported [38–41]. These spectroscopic features were also noted for CHX-SiNPs and CHX-SSiNPs (Fig. 1b). However, this spectroscopic information cannot be noticed for SiNPs and SSiNPs without a CHX loading. Thereby, encapsulation of CHX in CHX-SiNPs, CHX-SSiNPs was successfully developed through the designed method. Moreover, the thermal stability of the fabricated NPs was carried out through thermogravimetric analysis (TGA). The mass loss of every sample in the heating process from 21 °C to 80 °C displayed a small value, less than 0.7% (Fig. S1). Such a negligible mass loss strongly suggested that the synthesized NPs with and without a CHX loading were thermally stable in the testing temperature range.

3.3. Controlled drug release

To quantify the amount of CHX loaded in CHX-SiNPs and CHX-SSiNPs, 1 mL of 330 mg·L^{-1} CHX-SiNPs and CHX-SSiNPs were incubated at room temperature in PBS 10 mM at pH 9.0 for two weeks to achieve a maximum release of the loaded CHX owing to the complete degradation of silica in this condition [42]. Consequently, CHX loading was, respectively determined as 119.5 +/- 3.2 mg·L^{-1} and 120.8 +/- 22.7 mg·L^{-1} for CHX-SiNPs and CHX-SSiNPs for the amount of particles considered (330 mg·L^{-1} each sample). Therefore, the amount of CHX was determined to be 3.6 g·L^{-1} and 6.9 g·L^{-1}, respectively for the initial CHX-SiNPs (9.9 g·L^{-1}) and CHX-SSiNP (18.8 g·L^{-1}). The loading efficiency was calculated to be 23.7% for CHX-SiNP and 45.4% for CHX-SSiNP, considering that 15.2 g·L^{-1} were used for the synthesis. The higher loading efficiency determined for core-shell particles was explained by the larger particles and the protective effects of the outer shell favoring CHX loading. The cumulative release of CHX from CHX-SiNPs and CHX-SSiNPs was furthermore quantified in PBS buffer at pHs of 6.5, 7, 7.4, 8, and 8.5 within 30 h by UV-vis (Figs. 2a&b and S2). It was found that CHX release from CHX-SSiNPs was not impacted by the change of pH value at 6.5, 7, 7.4, 8, and 8.5, with a maximum CHX release lower than 14.0 mg·L^{-1}. A similar observation was made for CHX-SiNPs at pH of 6.5, 7.0, and 7.4, with a maximum release lower than 17.0 mg·L^{-1}. However, CHX-SiNPs at pH 8 and 8.5 released CHX of 89.1 +/- 3.8 mg·L^{-1} and 94.2 +/- 1.5 mg·L^{-1}, respectively, which were 4 - 5 fold higher than those at pH of 6.5, 7.0, and 7.4. Therefore, a CHX release from SiNPs can be regulated by alkaline pHs.

The different mechanisms of degradation of SiNPs and SSiNPs were further evaluated by TEM analysis. To this end, CHX-SiNPs and CHX-SSiNPs (0.2 g·L^{-1}) were incubated at 37 °C in PBS 10 mM at pH 6.5 and 8.5. After 2, 6, 8, and 24 h the samples were centrifuged, the pellet was washed once with DI water and subse-

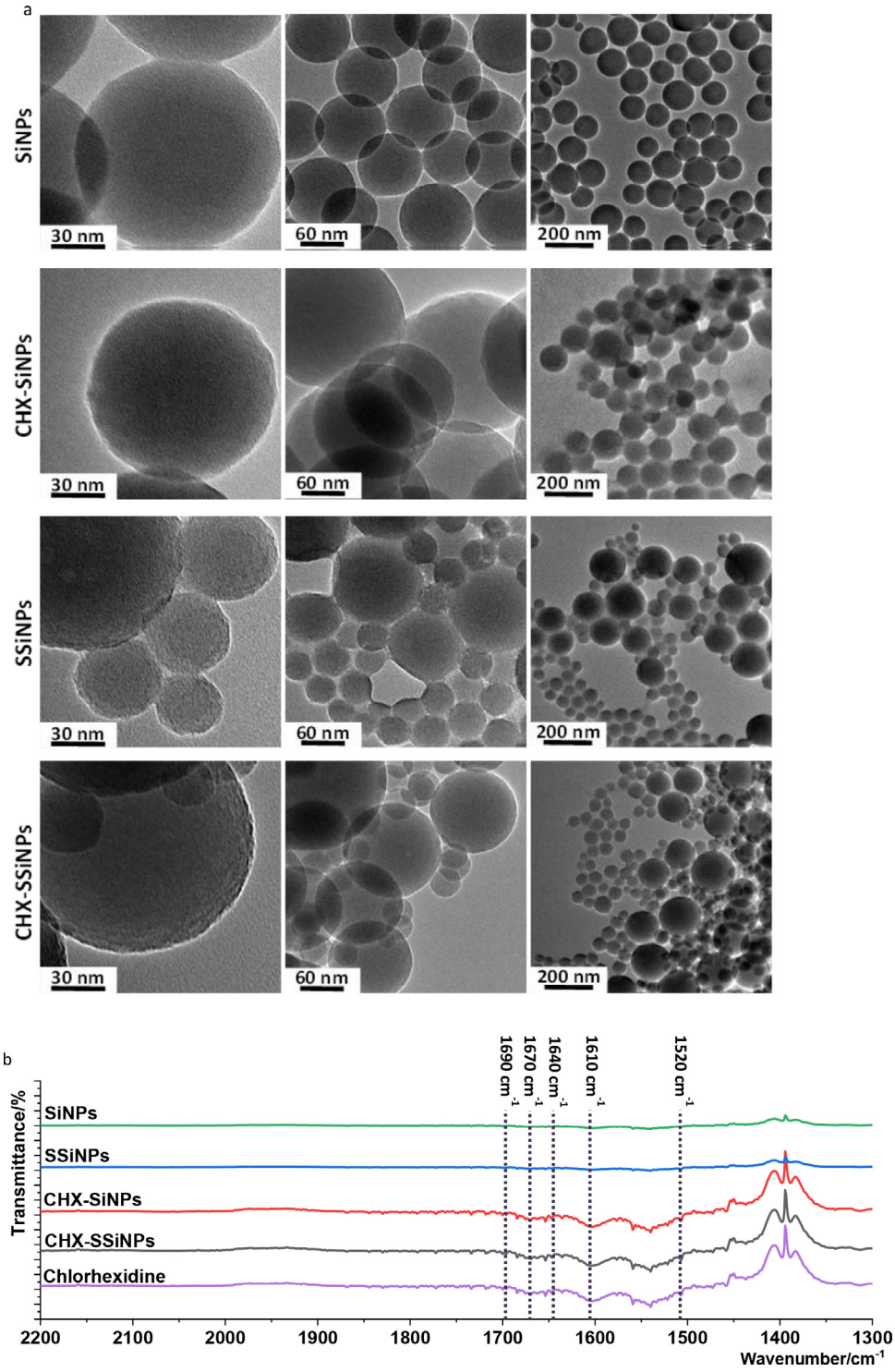

Fig. 1. Characterization of the fabricated NPs. (a) Morphological analysis of the fabricated silica nanoparticles through transmission electron microscopy (TEM). Representative micrographs are displayed for silica nanoparticles without and with a CHX loading. Every sample was imaged at least 10 times at different locations, and one representative image of every imaging is displayed. (b) Fourier-transform infrared spectra of SiNPs, CHX-SiNPs, SSiNPs, and CHX-SSiNPs. The band of N-H bending mode in secondary aromatic amine at 1520 cm^{-1}, C=N at 1610 cm^{-1}, characteristic bands of C=N stretching vibrations modes in 1690–1640 $cm^{-1,}$ and stretching vibrations of C=C group in 1670–1626 cm^{-1} typically for CHX [38–41], are all observed for the fabricated CHX-SiNPs and CHX-SSiNPs, but not for SiNPs and SSiNPs, suggesting a successful loading of CHX into CHX-SiNPs, CHX-SSiNPs. Every sample was analyzed five times, and similar results were obtained. One set of measurements is shown.

quently analyzed by TEM considering the NPs integrity as degradation parameter. As shown in Fig. 3a, a clear change in morphology after 2 h at pH 8.5 was observed for CHX-SiNPs, confirming the drug release test. After 8 h and more evident after 24 h, the remaining structures reorganized themselves by forming large silica deposits of a slight resemblance of spherical shape. CHX-SiNPs showed the typical hollowing mechanism described by Park et al. and caused by the etching of the silica matrix under alkaline conditions [43]. The mechanism was particularly evident at pH 6.5, at which the small pores, observed after 2 and 6 h, merged to form

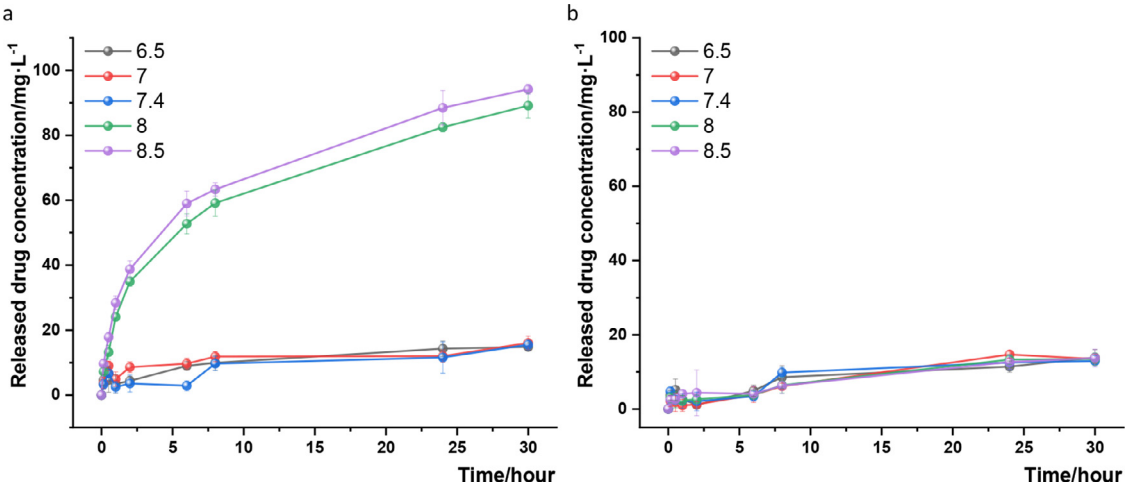

Fig. 2. Analysis of pH-regulated CHX release from CHX-loaded SiNPs and SSiNPs at different pH values. Cumulative CHX *in vitro* release from CHX-loaded SiNPs (a) and SSiNPs (b) at pH 6.5, 7, 7.4, 8 and 8.5 at 37 °C°C. Three independent experiments were performed. One set of measurements is shown. Data are expressed as mean +/- standard deviation ($n = 3$).

hollowed structures prolonging the incubation. The degradation of CHX-SSiNPs at different pHs can be noticed in Fig. 3b. In this case, two different behaviors can be observed for the small and the large particles. Indeed, the smaller particles underwent Ostwald ripening after only 2 h at pH 6.5 and 8.5, leading to reorganization of the material to a more energetically stable state, and yielding hollowing particles [44]. Reasonably, the low drug release observed for CHX-SSiNPs was related to the low amount of CHX loaded in such small particles compared to the amount of drug hosted in the larger population, which did not degrade easily and were still observed even after 24 h at pH 8.5. For the large core-shell-particles, we observed the formation of small pores instead after 2 h at pH 8.5. Considering the different degradation behaviors of smaller and larger particles of the CHX-SSiNP, we concluded that the different release measured between core-shell-SiNPs and core-SiNPs is related to higher content of CHX in the larger particles, which were more resistant to degradation even at alkaline pH. Moreover, it should be considered that the charged silanes forming the shell (THPMP and APTMS) could potentially interact with CHX to hinder its release in the surrounding environment.

3.4. Antibacterial activity

The pH-regulated antibacterial activity of CHX-SiNPs and CHX-SSiNPs was investigated against *Escherichia coli* (Gram-negative) and *Staphylococcus aureus* (Gram-positive), two wound infection-associated pathogens (Fig. 4). The antibacterial activity of CHX-SiNPs and CHX-SSiNPs was first qualitatively analyzed with agar plates having pH at 6.5, 7.0, 7.4, 8.0, or 8.5, using 500 mg·L^{-1} CHX solution as a positive control. The bacterial growth inhibition zones were distinctively observed at pH 8.0 and 8.5 for both tested strains after applying 10 µL 330 mg·L^{-1} CHX-SiNPs (*circa.* 119.5 mg·L^{-1} of CHX). In contrast, no inhibition zone was detected for CHX-SSiNPs (10 µL of 330 mg·L^{-1} CHX-SSiNPs containing *circa* 120.8 mg·L^{-1} of CHX) (Fig. 4a&c). Furthermore, we performed quantitative antibacterial analysis against *E. coli* (Figs. 4b and S3 a-c) and *S. aureus* (Figs. 4d and S4 a-c) at various pH values. We observed significantly fewer viable bacterial cells after incubation with CHX-SiNPs at pH 8.0 and 8.5 (Fig. 4), which cannot be noticed at pH 6.5, 7.0, and 7.4 (Figs. S3 a-c and S4 a-c). At pH 8.0, about 2-lg reduction of viable cells was observed after incubation with CHX-SiNPs (*E. coli*: 6.1 +/- 1.8 × 10^3 CFU·mL^{-1}, and *S. aureus*: 11.5 +/- 1.4 × 10^3 CFU·mL^{-1}) compared with the negative controls (*E. coli*: 2.0 +/- 0.1 × 10^6 CFU·mL^{-1}, and *S. aureus*: 4.0 +/- 0.1 × 10^6 CFU·mL^{-1}) (Fig. 4 b&d). At pH 8.5, roughly 3-lg reduction of viable cells was found after incubation with CHX-SiNPs (*E. coli*: 2.6 +/- 1.0 × 10^3 CFU·mL^{-1}, and *S. aureus*: 2.4 +/- 0.6 × 10^3 CFU·mL^{-1}) compared with the negative controls (*E. coli*: 1.9 +/- 0.1 × 10^6 CFU·mL^{-1}, and *S. aureus*: 3.6 +/- 0.1 × 10^6 CFU·mL^{-1}) (Fig. 4 b&d). Therefore, the fabricated CHX-SiNPs displayed a significant *in vitro* antibacterial activity against both Gram-negative and -positive pathogens at alkaline conditions.

Alginate-based wound dressings are particularly attractive due to their favorable properties, such as biocompatibility and low cytotoxicity. Alginate can easily formulate NPs or active molecules to gain additional functions (*i.e.*, favor wound healing, prevention, and treating bacterial contamination) [45–47]. To simplify the evaluation of the SiNPs embedded alginate dressing, the pH-responsive SiNPs were loaded with a dye (fluorescein isothiocyanate, FITC) instead of CHX, allowing an appropriate visualization of the particles inside the hydrogel matrix (FITC-SiNPs@AH). A confocal microscope was used to evaluate the distribution of the labeled core-SiNPs (FITC-SiNPs) inside the alginate dressing (Fig. 5a&b). The undesired leakage of the particles from the matrix was evaluated by immersing FITC-SiNPs@AH in water for 2 h. No fluorescent signal was detected in the supernatant, indicating that the alginate matrix of silica particles was well-retained, likely due to the formation of hydrogen bonds between the available hydroxyl group on the NPs surface and the carboxyl groups on the alginate chains. The pH sensitivity of the SiNPs embedded in the alginate matrix was evaluated by fluorescent spectroscopies through immersing the FITC-SiNPs@AH in PBS at pH 6.0, 7.0, and 8.0 (Table S1). After of incubation of 2 h, the fluorescent signal of the supernatants was measured spectrophotometrically. Given the signal measured for the amount of FITC-SiNPs initially added to the hydrogel at every pH as 100%, the average ($n = 3$) relative amount of FITC released from FITC-SiNPs@AH at the different pHs was calculated to be 78% at pH 8.0. In contrast, only 6 and 10% were released at pH 7.0 and 6.0, respectively. The effect of pH in determining the particle degradation was observed even by confocal microscopic analysis. The number of fluorescent FITC-SiNPs decreases remarkably at pH 8.0, confirming the pH-dependent degradation of SiNPs even once embedded into the hydrogel matrix and proving its applicability as a wound dressing (Fig. 5b).

To mimic a clinic situation of wound infection, *ex vivo* human skin was utilized herein to create an artificial wound. After a

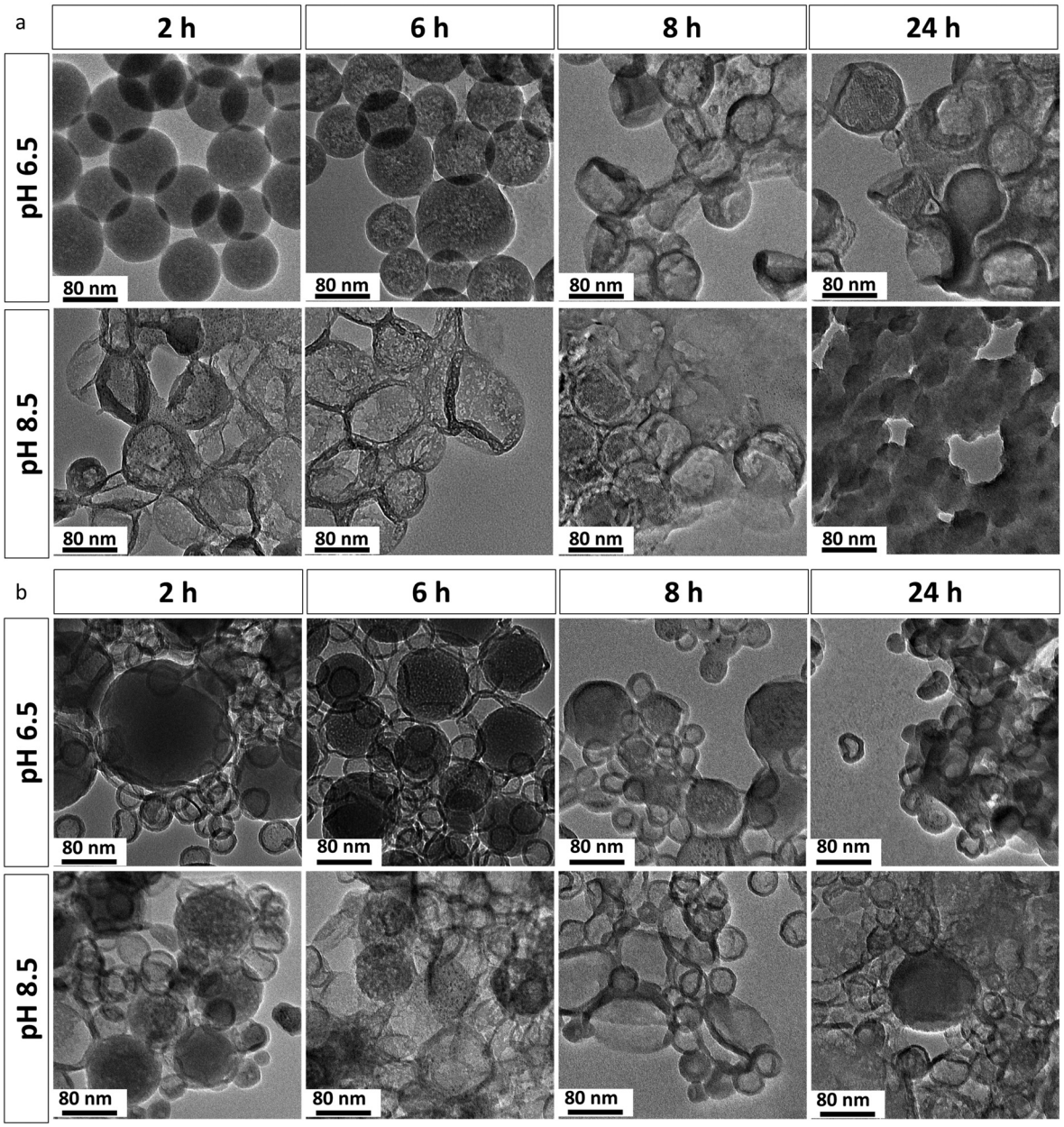

Fig. 3. CHX release mechanism regulated by pH was analyzed by exploiting TEM toward CHX-SiNPs (a) and CHX-SSiNPs (b). The two different NPs were immersed in PBS buffers of pH 6.5 and 8.5, respectively, for 2, 6, 8, and 24 h. After the degradation for a given time, the sample was centrifuged and then prepared for further TEM observation.

subsequent intentional bacterial infection on artificial wounds for 24 h (wound pH in the range of 8.5–9.0, Fig. S5), CHX-SiNPs and CHX-SSiNPs were applied either as suspension or in the formulated alginate hydrogel (SiNPs, SSiNPs, CHX-SiNPs@AH, and CHX-SSiNPs@AH). After treatment of two hours, the wound was transferred to a tube of 5 mL PBS and subsequently ultrasonicated before counting. Antibacterial activity was observed for CHX-SiNPs and CHX-SiNPs@AH (Fig. 5 c&d), respectively manifesting 4-lg and 3-lg reduction of viable cells compared with the negative control. Moreover, similar antibacterial efficacies of CHX-SiNPs and CHX-SiNPs@AH were observed towards *S. aureus* (Fig. 5 c&d). This *ex vivo* study on infected human skin proved the efficiency of the pH-regulated release of the bactericidal compound from CHX-SiNPs even when formulated as a smart pH-responsive wound dressing.

Furthermore, histological staining was applied to evaluate the antibacterial activity of CHX-SiNPs and the AH-formulated CHX-SiNPs on the artificially infected wounds (Fig. 6). *E. coli* suspension was loaded onto the artificial wounds and grew for three days, and the infected wounds displayed an alkaline pH in the range of 8.5–9.0 (Fig. S5). Subsequently, CHX-SiNPs and CHX-SiNPs@AH were applied to the infected wounds for two hours. The bacterial colonies (black clusters) can be observed on the infected wounds without treatments. In contrast, no bacterial clusters were observed on the treated wounds, likely due to the triggered CHX release from CHX-SiNPs at alkaline pH. Thereby, the fabricated CHX-SiNPs can effectively eliminate bacteria on the infected wounds based on the qualitative observation (Fig. 6).

3.5. Cytotoxicity

The fabricated pH-triggered SiNPs could restrain CHX release at acidic or neutral pH unless reaching an alkaline pH (Fig. 2),

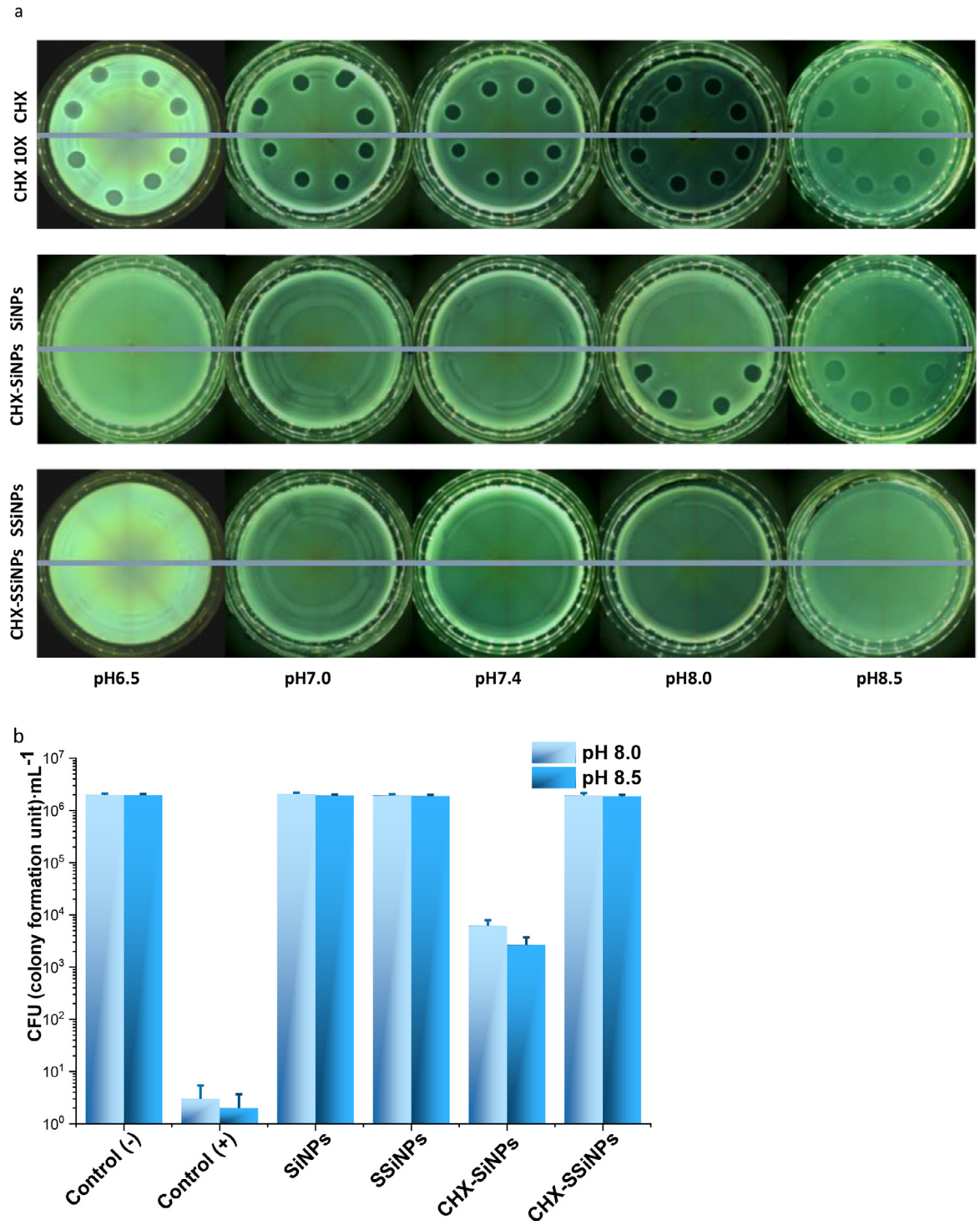

Fig 4. *In vitro* antibacterial efficacies of NPs at various pHs. Inhibition of bacterial growth was performed towards Gram-negative bacteria *E. coli* by qualitative analysis (a) and quantitative analysis (b), and towards Gram-positive bacteria *S. aureus* by qualitative analysis (c) and quantitative analysis (d). (a)&(c) 500 mg·L^{-1} CHX solution and its 10 times diluted solution were applied as positive controls, and SiNPs and SSiNPs without a CHX loading were applied as negative controls. 10 µL CHX-SiNPs and CHX-SSiNPs and positive and negative controls were plotted four times on agar plates (of pH 6.5, 7.0, 7.4, 8.0, and 8.5), on which 200 µL bacterial suspension (OD_{600} 0.01) was sprayed. (b)&(d) Inhibition of bacterial growth was quantitatively analyzed at pH 8.0 and pH 8.5 by applying SiNPs, SSiNPs, CHX-SiNPs, and CHX-SSiNPs. The untreated bacterial suspensions at both pHs were the negative control. The bacterial suspension incubated with 500 mg·L^{-1} CHX was the positive control for the analysis at every pH condition. The analysis was performed with three replicates, and every replicate was plated with three technical repeats for counting to yield average values and error bars. A significant difference in every graph was noticed in all tests from CHX-SiNPs towards negative and positive control, SiNPs, SSiNPs, and CHX-SSiNPs. Student's *t*-test ($p < 0.05$) was performed for statistical analysis.

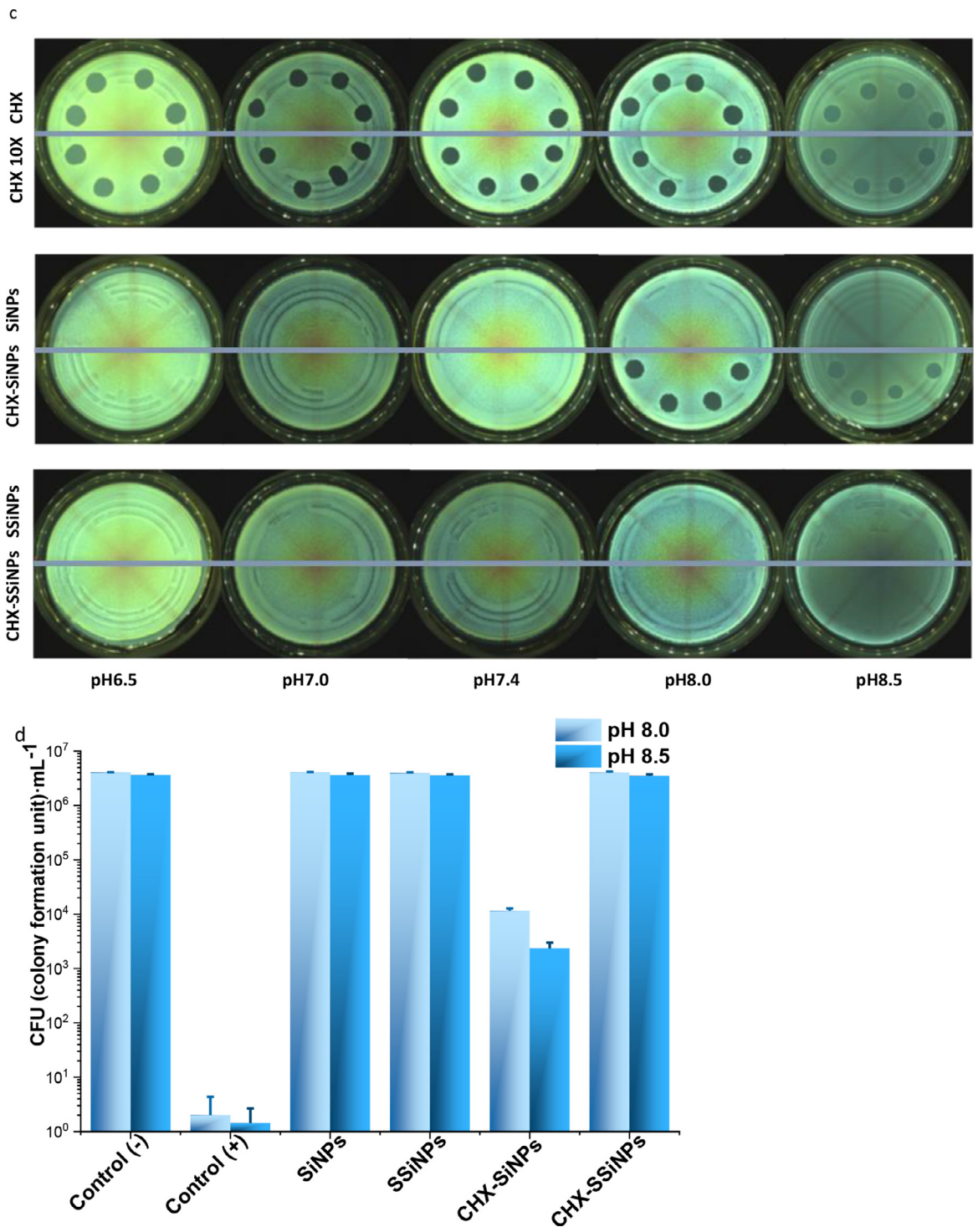

Fig 4. Continued

a similar pH condition found on chronic wounds [9]. The cytotoxicity of the fabricated NPs towards normal human dermal fibroblasts (nHDFs) was evaluated using a previously reported method [48,49]. CHX-SiNPs of different dilutions were incubated with nHDFs in DMEM (Dulbecco's Modified Eagle Medium) with 1% penicillin/streptomycin/neomycin (PSN) for 24 h at pH 7.4, 8.0, and 8.5. The viable nHDFs were evaluated by applying the MTS [(3-(4,5-Dimethylthiazol-2-yl)-5-(3-carboxymethoxyphenyl)-2-(4-sulfophenyl)-2H-tetrazolium] assay, as described in experimental procedures. The cytotoxicity of CHX-SiNPs was displayed as a comparison to positive and negative controls at different pH. The cytotoxic cut-off was set as 70% viability of the cells in the negative control. The CHX-loaded SiNPs at the evaluated pHs showed more than 85% cell viability (Fig. 7 a, b&c). Thereby, the cytotoxicity was not noticed for the CHX loaded SiNPs within the tested concentrations. Moreover, the cytotoxicity of CHX-SiNPs displayed a better performance when compared to the clinic CHX solution (20 $g{\cdot}L^{-1}$) [50].

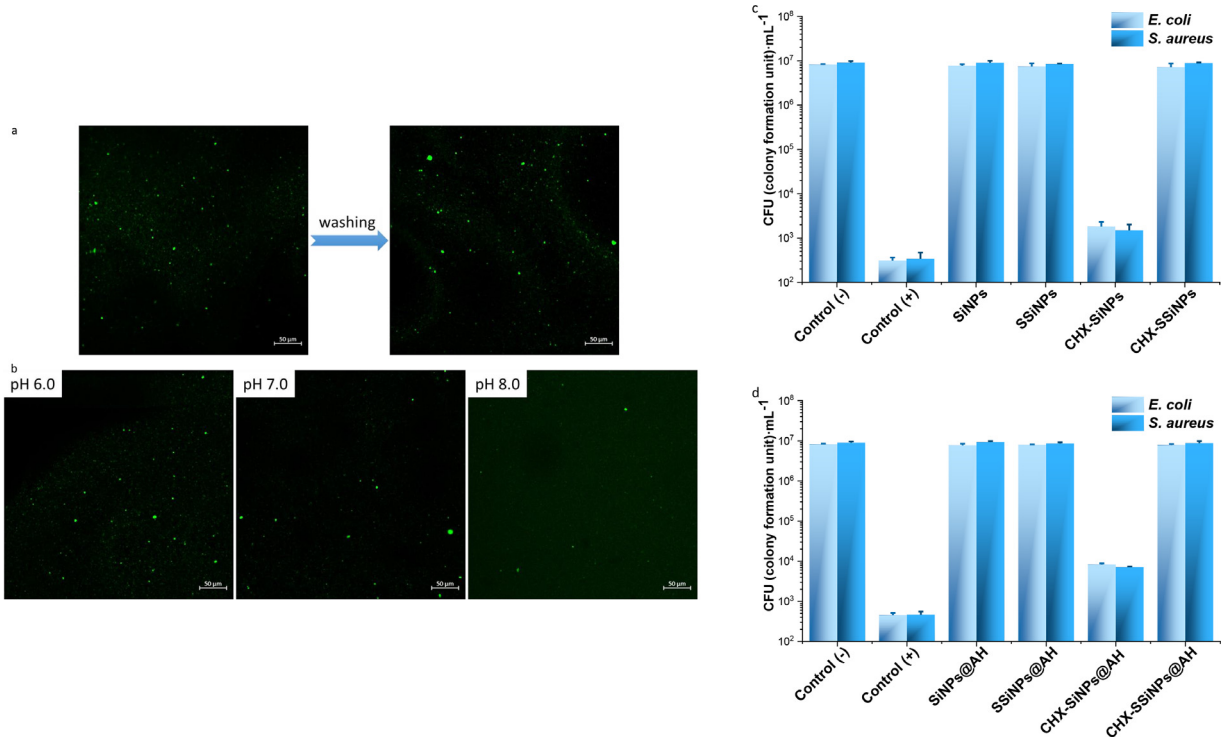

Fig. 5. Antibacterial efficacy analysis on artificial wound infections towards NPs and NPs formulated by alginate hydrogel (AH). (a) Confocal microscopic analysis of the labeled core-SiNPs embedded in the alginate hydrogel. FITC-SiNPs@AH before and after washing with water confirms the retention of the particles by the alginate matrix. (b) A confocal microscope was exploited to image the FITC-SiNPs in the hydrogel after immersing in PBS at pH 6.0, 7.0, and 8.0. The fluorescence decay of FITC-SiNPs in the hydrogel after immersing in PBS at alkaline pH proved the preservation of the pH-triggered degradation of SiNPs in alkaline conditions. Scale bar 50 µm. Artificial human wounds were utilized to evaluate the antibacterial efficacies of the fabricated NPs (c) and their alginate formulated forms (d). The artificial wounds were infected by 862 500 +/- 74 106 CFU·mL^{-1} *E.coli* (c)&(d) and 917 500 +/- 77 190 CFU·mL^{-1} *S. aureus* (c)&(d). 500 mg·L^{-1} CHX solution was used as the positive control, and the infected wounds were treated with PBS buffer as a negative control; all the wounds except the wound surface were kept immersed in DMEM containing 10% foetal calf serum (FCS) during experiments. NPs and AH-formulated NPs were applied to the infected sites and incubated for 2 h at 37 °C. The analysis was performed with three replicates. There was a significant difference in c from CHX-SiNPs compared to the negative and positive control, SiNPs, SSiNPs, and CHX-SSiNPs, towards each bacterial strain. A significant difference towards each bacterial strain in d was noticed from CHX-SiNPs@AH towards negative and positive control, SiNPs@AH, SSiNPs@AH, and CHX-SSiNPs@AH. Student's *t*-test ($p < 0.05$) was performed for statistical analysis.

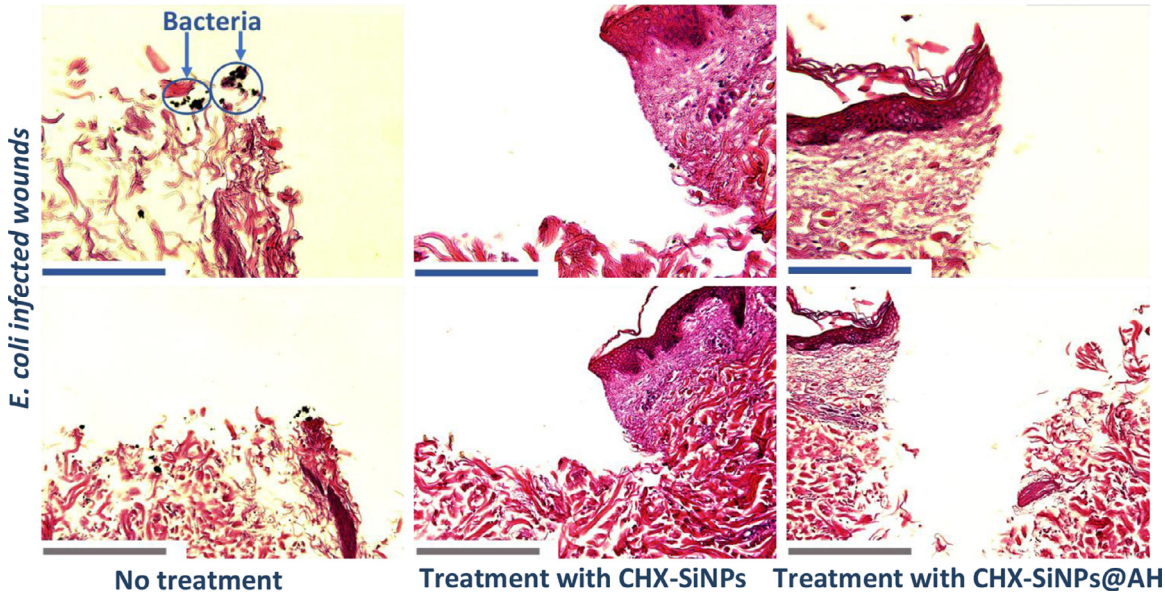

Fig. 6. Histological staining analysis of targeted treatment efficacy. Artificial wounds were infected with *E. coli* for three days. The infected wounds were subsequently treated with CHX-SiNPs and CHX-SiNPs@AH. Scale bar: 145 µm for blue ones and 290 µm for grey ones.

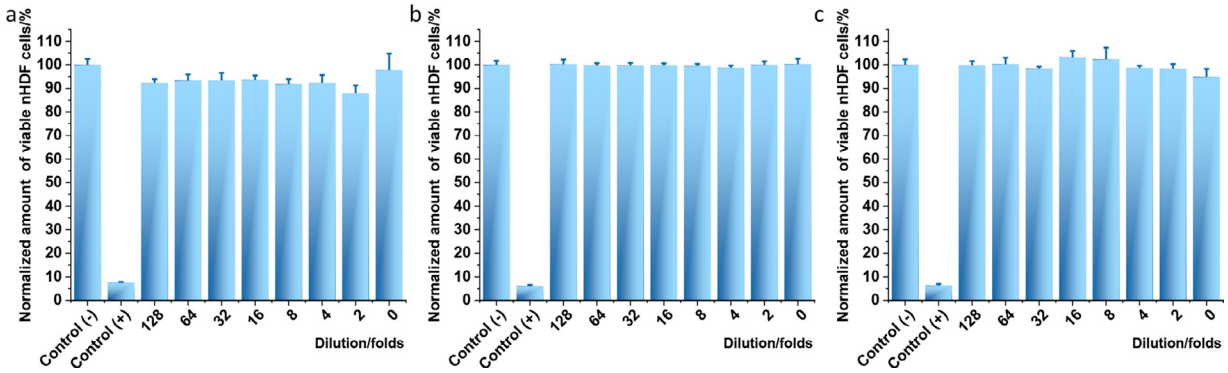

Fig. 7. Cytotoxicity analysis of CHX-loaded SiNPs. Viable normal human dermal fibroblasts (nHDFs) after their incubation of 24 h at 37 °C with CHX-loaded SiNPs in DMEM containing 1% penicillin/streptomycin/neomycin (PSN) at pH 7.4 (a), 8.0 (b) and 8.5 (c). Error bars meant the standard deviations generated from 9 measurements, and no cytotoxicity was determined for all samples.

4. Conclusions

This proof of concept work depicted pH as a non-invasive stimulus to on-demand deliver antimicrobials loaded in SiNPs at an alkaline condition, usually identified on chronic wounds. The difference of released drugs between an alkaline condition and a neutral/an acidic condition can be higher than 5 folds after a CHX release for 2 h and 30 h. Consequently, effective inhibition of bacterial growth was noticed in line with qualitative analysis on agar plates at various pH values. Assisted by *ex vivo* human skin, a quantitative analysis of the antibacterial efficacy of SiNPs and SSiNPs loaded with CHX on infected wounds was achieved. Nearly a 4-lg reduction of viable bacterial cells on infected wounds was hereupon observed for CHX-SiNPs and nearly a 3-lg reduction for CHX-SiNPs@AH, compared with the non-treated ones. Several examples have been reported previously on using nanomaterials and hydrogels to achieve the controlled release of antimicrobials in an acidic environment [51,52]. In contrast, scarce work has been found reporting the release in alkaline conditions, and at the same time limited release in acidic conditions. Further, it appears difficult to limit the interference of other factors with the pH-responsiveness such as the ionic strength [53]. This highlights the advantage of the proposed SiNPs, with which we achieved a rapid release of almost 90% of the loaded CHX at pH over 8 unlike a release of 20% achieved at pH below 8. Moreover, given that the mechanism of drug release was only related to the degradation of the silica matrix in an alkaline environment, the effect of other parameters on drug release was minimized. This study showcased non-cytotoxic SiNPs can be utilized to on-demand deliver antibacterial agents onto infected wounds without the intervention of external stimulus, thereby permitting an effective killing of bacteria on infected wounds. Exploiting an *ex vivo* human skin in this study can mimic a real situation of clinic infections on wounds, bringing this study clinic potential to treat chronic wounds.

Declaration of Competing Interest

The authors declare no competing financial interest.

CRediT authorship contribution statement

Fei Pan: Conceptualization, Methodology, Software, Validation, Formal analysis, Investigation, Visualization, Supervision, Project administration, Writing – original draft, Writing – review & editing. **Giorgia Giovannini:** Conceptualization, Methodology, Validation, Formal analysis, Investigation, Visualization, Project administration, Writing – original draft, Writing – review & editing. **Sixuan Zhang:** Methodology, Investigation, Validation. **Stefanie Altenried:** Methodology, Validation, Investigation. **Flavia Zuber:** Methodology, Validation, Investigation. **Qian Chen:** Conceptualization, Methodology, Validation, Writing – review & editing. **Luciano F. Boesel:** Supervision, Funding acquisition, Writing – review & editing. **Qun Ren:** Conceptualization, Methodology, Validation, Investigation, Supervision, Project administration, Writing – review & editing.

Acknowledgments

The authors would like to thank Luzia Wiesli and Lucia Hirschi for their assistance in preparing agar plates of different pH values and Prof. Jörg Grünert at the Cantonal Hospital St. Gallen, Switzerland, for providing *ex vivo* human skin samples. FP acknowledges Berna Neidhart for the insightful scientific discussions. GG and LFB acknowledge the support from the Novartis Research Foundation (project “LightLoop”).

Supplementary materials

Supplementary material associated with this article can be found, in the online version, at doi:10.1016/j.actbio.2022.04.009.

References

[1] H. Yousef, M. Alhajj, S. Sharma, Anatomy Skin, Epidermis, StatPearls Publishing, Treasure Island (FL), 2020 (Integument).
[2] E.M. Tottoli, R. Dorati, I. Genta, E. Chiesa, S. Pisani, B. Conti, Skin wound healing process and new emerging technologies for skin wound care and regeneration, Pharmaceutics 12 (8) (2020) 735.
[3] J. Hurlow, K. Couch, K. Laforet, L. Bolton, D. Metcalf, P. Bowler, Clinical biofilms: a challenging frontier in wound care, Adv. Wound Care 4 (5) (2015) 295–301.
[4] F. Pan, S. Altenried, M. Liu, D. Hegemann, E. Bülbül, J. Moeller, W.W. Schmahl, K. Maniura-Weber, Q. Ren, A nanolayer coating on polydimethylsiloxane surfaces enables a mechanistic study of bacterial adhesion influenced by material surface physicochemistry, Mater. Horiz. 7 (1) (2020) 93–103.
[5] F. Pan, A. Amarjargal, S. Altenried, M. Liu, F. Zuber, Z. Zeng, R.M. Rossi, K. Maniura-Weber, Q. Ren, Bioresponsive hybrid nanofibers enable controlled drug delivery through glass transition switching at physiological temperature, ACS Appl. Bio Mater. 4 (5) (2021) 4271–4279.
[6] F. Werdin, M. Tenenhaus, H.O. Rennekampff, Chronic wound care, Lancet N. Am. Ed. 372 (9653) (2008) 1860–1862.
[7] World Health Organization, Global action plan on antimicrobial resistance, World Health Organization (2015) Geneva.
[8] World Health Organization, Global antimicrobial resistance and use surveillance system (GLASS) report: 2021, (2021).
[9] G. Gethin, The significance of surface pH in chronic wounds, Wounds UK 3 (3) (2007) 52.
[10] J.P. Gleeson, S.M. Ryan, D.J. Brayden, Oral delivery strategies for nutraceuticals: delivery vehicles and absorption enhancers, Trends Food Sci. Technol. 53 (2016) 90–101.
[11] A. Tivnan, W.S. Orr, V. Gubala, R. Nooney, D.E. Williams, C. McDonagh, S. Prenter, H. Harvey, R. Domingo-Fernández, I.M. Bray, Inhibition of neuroblastoma tumor growth by targeted delivery of microRNA-34a using anti-disialoganglioside GD 2 coated nanoparticles, PLoS One 7 (5) (2012) e38129.

[12] L.H. Chuah, C.J. Roberts, N. Billa, S. Abdullah, R. Rosli, Cellular uptake and anticancer effects of mucoadhesive curcumin-containing chitosan nanoparticles, Colloids Surf. B 116 (2014) 228–236.
[13] H. Amekyeh, N. Billa, C. Roberts, Correlating gastric emptying of amphotericin B and paracetamol solid lipid nanoparticles with changes in particle surface chemistry, Int. J. Pharm. 517 (1-2) (2017) 42–49.
[14] R. Singh, J.W. Lillard Jr, Nanoparticle-based targeted drug delivery, Exp. Mol. Pathol. 86 (3) (2009) 215–223.
[15] R. Xie, Y. Li, L.Y. Chu, Preparation of thermo-responsive gating membranes with controllable response temperature, J. Membr. Sci. 289 (1-2) (2007) 76–85.
[16] M. Wang, Q.F. An, L.G. Wu, J.X. Mo, C.J. Gao, Preparation of pH-responsive phenolphthalein poly (ether sulfone) membrane by redox-graft pore-filling polymerization technique, J. Membr. Sci. 287 (2) (2007) 257–263.
[17] X.Z. Zhang, P.J. Lewis, C.C. Chu, Fabrication and characterization of a smart drug delivery system: microsphere in hydrogel, Biomaterials 26 (16) (2005) 3299–3309.
[18] J.T. Keurentjes, M.F. Kemmere, H. Bruinewoud, M.A. Vertommen, S.A. Rovers, R. Hoogenboom, L.F. Stemkens, F.L. Péters, N.J. Tielen, D.T. van Asseldonk, Externally triggered glass transi-tion switch for localized on-demand drug delivery, Angew. Chem. Int. Ed. 48 (52) (2009) 9867–9870.
[19] R. Langer, Drug delivery and targeting, Nature 392 (1998) 5–10.
[20] F. Barandeh, P.L. Nguyen, R. Kumar, G.J. Iacobucci, M.L. Kuznicki, A. Kosterman, E.J. Bergey, P.N. Prasad, S. Gunawardena, Organically modified silica nanoparticles are biocompatible and can be targeted to neurons *in vivo*, PLoS One 7 (1) (2012) e29424.
[21] G. Giovannini, P. Warncke, D. Fischer, O. Stranik, A.J. Hall, V. Gubala, Improving colloidal stability of silica nanoparticles when stored in responsive gel: application and toxicity study, Nanotoxicology 12 (5) (2018) 407–422.
[22] G. Giovaninni, C.J. Moore, A.J. Hall, H.J. Byrne, V. Gubala, pH-Dependent silica nanoparticle dissolution and cargo release, Colloids Surf. B 169 (2018) 242–248.
[23] V. Gubala, G. Giovannini, F. Kunc, M.P. Monopoli, C.J. Moore, Dye-doped silica nanoparticles: synthesis, surface chemistry and bioapplications, Cancer Nanotechnol. 11 (1) (2020) 1–43.
[24] L. McCusker, F. Liebau, G. Engelhardt, Nomenclature of structural and compositional characteristics of ordered microporous and mesoporous materials with inorganic hosts (IUPAC Recommendations 2001), Pure Appl. Chem. 73 (2) (2001) 381–394.
[25] M. Thommes, K. Kaneko, A.V. Neimark, J.P. Olivier, F. Rodriguez-Reinoso, J. Rouquerol, K.S. Sing, Physisorption of gases, with special reference to the evaluation of surface area and pore size distribution (IUPAC Technical Report), Pure Appl. Chem. 87 (9-10) (2015) 1051–1069.
[26] O. Mimoz, J.C. Lucet, T. Kerforne, J. Pascal, B. Souweine, V. Goudet, A. Mercat, L. Bouadma, S. Lasocki, S. Alfandari, Skin antisepsis with chlorhexidine–alcohol versus povidone iodine–alcohol, with and without skin scrubbing, for prevention of intravascular-catheter-related infection (CLEAN): an open-label, multicentre, randomised, controlled, two-by-two factorial trial, Lancet N. Am. Ed. 386 (10008) (2015) 2069–2077.
[27] A. Rosenberg, S. Alatary, A. Peterson, Safety and efficacy of the antiseptic chlorhexidine gluconate, Surg. Gynecol. Obstet. 143 (5) (1976) 789–792.
[28] G. Giovannini, F. De Angelis, Novel electro-magnetophoretic separation method for the highly sensitive detection of analytes, Nanoscale Horiz. 5 (1) (2020) 95–101.
[29] S. Schmidt-Emrich, P. Stiefel, P. Rupper, H. Katzenmeier, C. Amberg, K. Maniura-Weber, Q. Ren, Rapid assay to assess bacterial adhesion on textiles, Materials 9 (4) (2016) 249.
[30] F. Pan, S. Altenried, F. Zuber, R.S. Wagner, Y.H. Su, M. Rottmar, K. Maniura-Weber, Q. Ren, Photo-activated titanium surface confers time dependent bactericidal activity towards Gram positive and negative bacteria, Colloids Surf. B 206 (2021) 111940.
[31] M.A. Andersson, L.B. Madsen, A. Schmidtchen, M. Puthia, Development of an experimental *ex vivo* wound model to evaluate antimicrobial efficacy of topical formulations, Int. J. Mol. Sci. 22 (9) (2021) 5045.
[32] S.C. Becerra, D.C. Roy, C.J. Sanchez, R.J. Christy, D.M. Burmeister, An optimized staining technique for the detection of Gram positive and Gram negative bacteria within tissue, BMC Res. Notes 9 (2016) 216 216.
[33] G. Jin, M.P. Prabhakaran, D. Kai, S.K. Annamalai, K.D. Arunachalam, S. Ramakrishna, Tissue engineered plant extracts as nanofibrous wound dressing, Biomaterials 34 (3) (2013) 724–734.
[34] H. Fullriede, P. Abendroth, N. Ehlert, K. Doll, J. Schäske, A. Winkel, S.N. Stumpp, M. Stiesch, P. Behrens, pH-responsive release of chlorhexidine from modified nanoporous silica nanoparticles for dental applications, BioNanoMaterials 17 (1-2) (2016) 59–72.
[35] F.J. Arriagada, K. Osseo-Asare, Controlled hydrolysis of tetraethoxysilane in a nonionic water-in-oil microemulsion: a statistical model of silica nucleation, Colloids Surf. A 154 (3) (1999) 311–326.
[36] A.S. Joshi, P. Singh, I. Mijakovic, Interactions of gold and silver nanoparticles with bacterial biofilms: molecular interactions behind inhibition and resistance, Int. J. Mol. Sci. 21 (20) (2020) 7658.
[37] P. Zeng, A. Rao, T.S. Wiedmann, W. Bowles, Solubility properties of chlorhexidine salts, Drug Dev. Ind. Pharm. 35 (2) (2009) 172–176.
[38] D. Luo, S. Shahid, R.M. Wilson, M.J. Cattell, G.B. Sukhorukov, Novel formulation of chlorhexidine spheres and sustained release with multilayered encapsulation, ACS Appl. Mater. Interfaces 8 (20) (2016) 12652–12660.
[39] J.W. Gooch, A.W. Johnston, A.F. Johnston, Broad Spectrum Antimicrobial Purification Materials and Methods for Purifying Fluids, Google Patents, 2008.
[40] E. Taşal, M. Tanışlı, A comparison for application time of electrical discharge onto 3-acetamidocoumarin molecule, J. Mol. Liq. 221 (2016) 763–767.
[41] R.M. Silverstein, F.X. Webster, D.J. Kiemle, D.L. Bryce, Spectrometric Identification of Organic Compounds, 8 ed., Wiley 2014.
[42] C.J. Moore, G. Giovannini, F. Kunc, A.J. Hall, V. Gubala, Overloading' fluorescent silica nanoparticles with dyes to improve biosensor performance, J. Mater. Chem. B 5 (28) (2017) 5564–5572.
[43] S.J. Park, Y.J. Kim, S.J. Park, Size-dependent shape evolution of silica nanoparticles into hollow structures, Langmuir 24 (21) (2008) 12134–12137.
[44] D.T. Nguyen, K.S. Kim, Self-development of hollow TiO2 nanoparticles by chemical conversion coupled with Ostwald ripening, Chem. Eng. J. 286 (2016) 266–271.
[45] C.M. Cleetus, F.A. Primo, G. Fregoso, N.L. Raveendran, J.C. Noveron, C.T. Spencer, C.V. Ramana, B. Joddar, Alginate hydrogels with embedded ZnO nanoparticles for wound healing therapy, Int. J. Nanomed. 15 (2020) 5097.
[46] D.A. Jankowska, M.B. Bannwarth, C. Schulenburg, G. Faccio, K. Maniura-Weber, R.M. Rossi, L. Scherer, M. Richter, L.F. Boesel, Simultaneous detection of pH value and glucose concentrations for wound monitoring applications, Biosens. Bioelectron. 87 (2017) 312–319.
[47] B.A. Aderibigbe, B. Buyana, Alginate in wound dressings, Pharmaceutics 10 (2) (2018) 42.
[48] N. Lewinski, V. Colvin, R. Drezek, Cytotoxicity of nanoparticles, Small 4 (1) (2008) 26–49.
[49] Z. Alhalili, J. Shapter, N. Hikmatul Auliya, B. Sandersonb, Investigation of the pH dependent cytotoxicity of paclitaxel conjugated gold nanoparticles, Pharm. Nanotechnol. 5 (2) (2017) 111–118.
[50] J.X. Liu, J. Werner, T. Kirsch, J.D. Zuckerman, M.S. Virk, Cytotoxicity evaluation of chlorhexidine gluconate on human fibroblasts, myoblasts, and osteoblasts, J. Bone Joint Infect. 3 (4) (2018) 165–172.
[51] Y. Zou, P. Wang, A. Zhang, Z. Qin, Y. Li, Y. Xianyu, H. Zhang, Covalent organic framework-incorporated nanofibrous membrane as an intelligent platform for wound dressing, ACS Appl. Mater. Interfaces 14 (7) (2022) 8680–8692.
[52] Y. Chen, Q. Zhao, J. Han, X. Lan, J. Che, M. Chen, X.J. Liang, X. Ma, Dual drug loaded pH-sensitive micelles for efficient bacterial infection treatment, Pharm. Res. (2022).
[53] P. Pino, S. Ronchetti, C. Mollea, M. Sangermano, B. Onida, F. Bosco, Whey proteins–zinc oxide bionanocomposite as antibacterial films, Pharmaceutics 13 (9) (2021) 1426.